Electronic Supplementary Material (ESI) for Inorganic Chemistry Frontiers.

Selective hydrogenation of CO_2 over a Ce promoted Cu-based catalyst confined by SBA-15

Xiaosong Hu,[a] *Chaoyue Zhao,*[a] *Qingxin Guan,**[a] *Xin Hu,*[a] *Wei Li,**[ab] *and Jun Chen*[ab]

[a] College of Chemistry, State Key Laboratory of Elemento-Organic Chemistry, Key Laboratory of Advanced Energy Materials Chemistry (Ministry of Education), Nankai University, Tianjin 300071, China

[b] Collaborative Innovation Center of Chemical Science and Engineering (Tianjin), Nankai University, Tianjin 300071, China

Corresponding Author

*E-mail: qingxinguan@nankai.edu.cn

*E-mail: weili@nankai.edu.cn

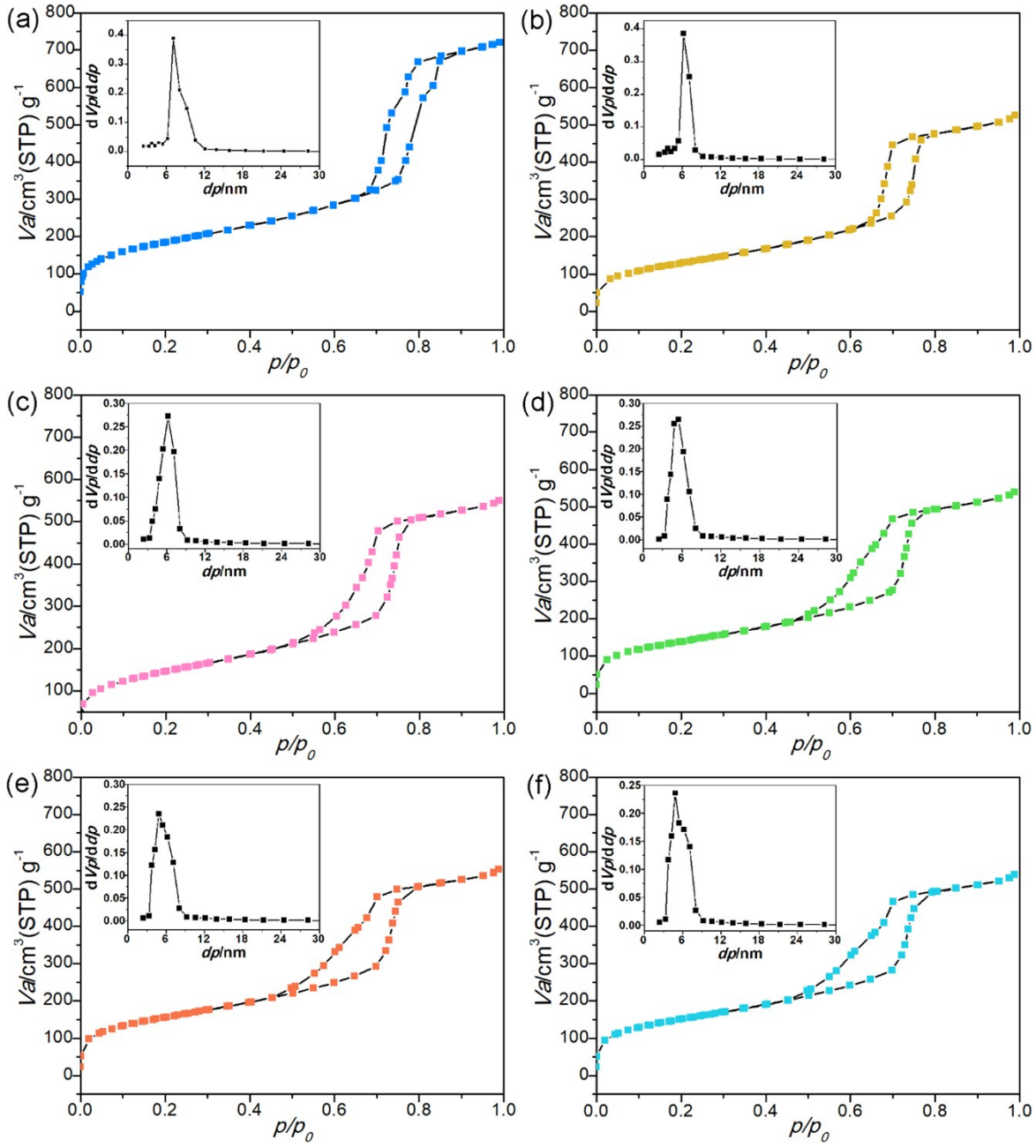

Fig. S1. N_2 adsorption-desorption isotherms and pore size distributions of different catalysts: (a) SBA-15; (b) $Cu_{0.5}Zn_{0.5}$/SBA-15; (c) $Cu_{0.5}Zn_{0.4}Ce_{0.1}$/SBA-15; (d) $Cu_{0.5}Zn_{0.25}Ce_{0.25}$/SBA-15; (e) $Cu_{0.5}Zn_{0.1}Ce_{0.4}$/SBA-15; (f) $Cu_{0.5}Ce_{0.5}$/SBA-15.

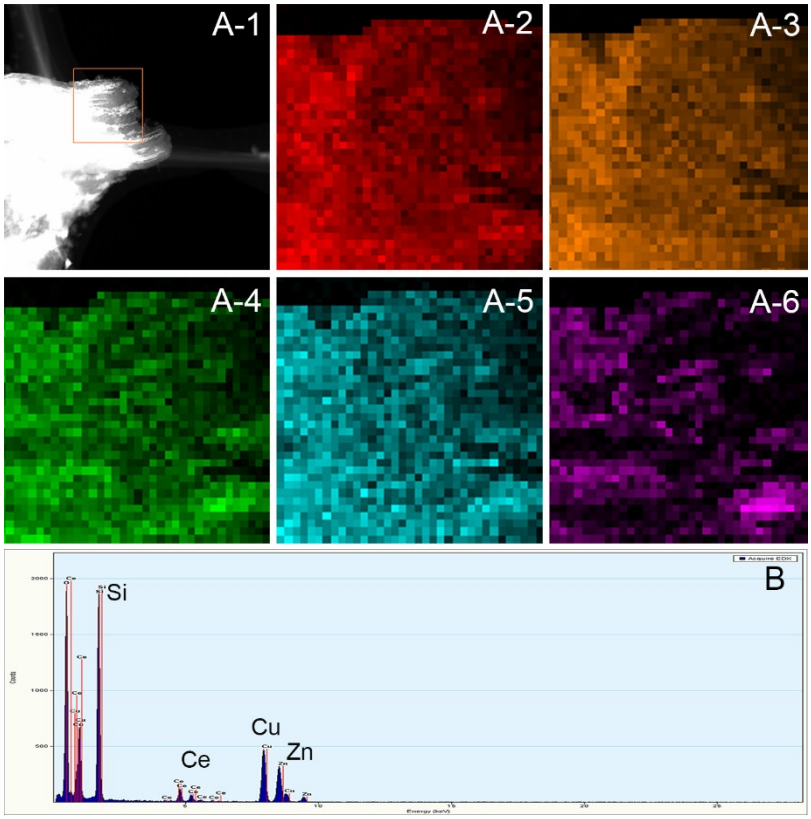

Fig. S2. STEM-Mapping (A) and EDX (B) of the reduced $Cu_{0.5}Zn_{0.4}Ce_{0.1}$/SBA-15: (A-1) STEM; (A-2) O; (A-3) Si; (A-4) Cu; (A-5) Zn; (A-6) Ce.

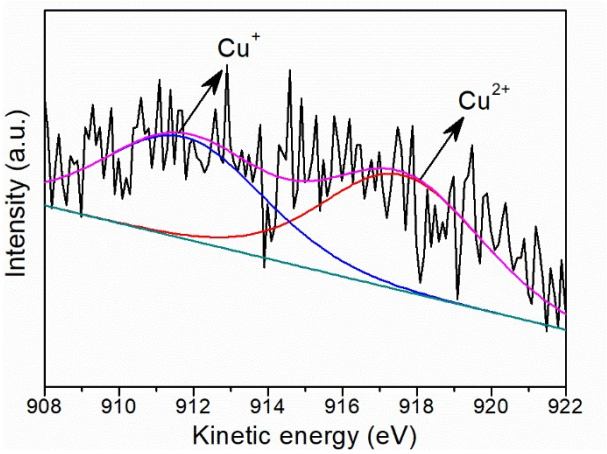

Fig. S3. XAES (X-ray auger spectra) of Cu LMM ($Cu_{0.5}Zn_{0.4}Ce_{0.1}$/SBA-15).

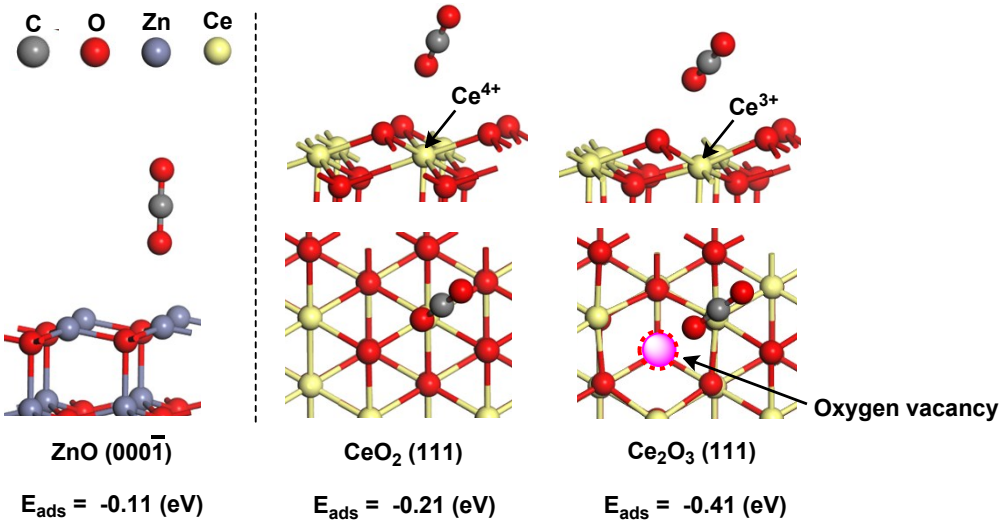

Fig. S4. Optimized adsorption structures and adsorption energies (E_{ads}) of CO_2 molecules on ZnO (0001), CeO_2 (111) and reduced CeO_2 (111) (with oxygen vacancies) surfaces. The values in electronvolts correspond to the adsorption energies of each adsorbate.

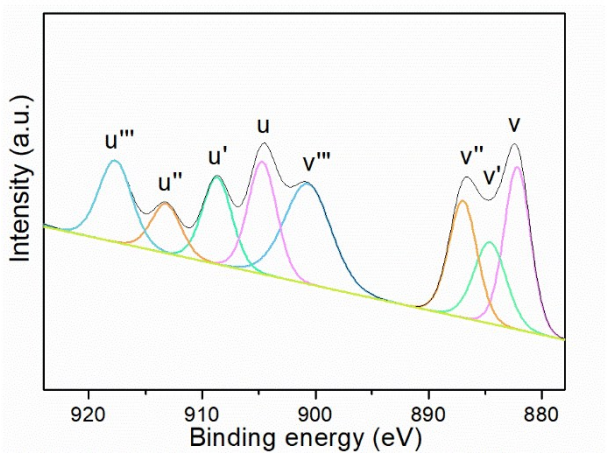

Fig. S5. XPS spectra for Ce 3d of the reduced $Cu_{0.5}Zn_{0.4}Ce_{0.1}$/SBA-15 catalyst.

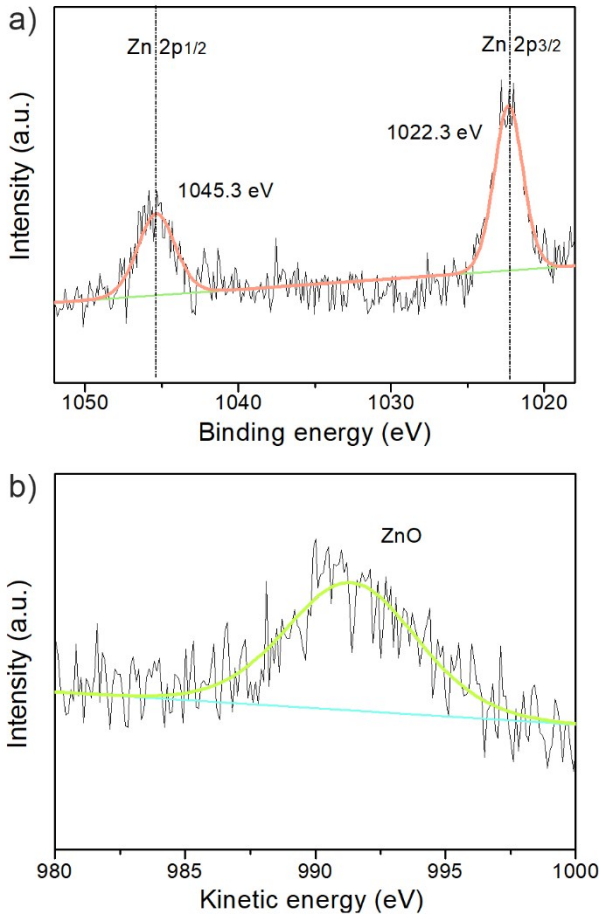

Fig. S6. (a) Zn 2p XPS spectrum and (b) Zn LMM XAES spectrum of the reduced $Cu_{0.5}Zn_{0.4}Ce_{0.1}$/SBA-15 catalyst.

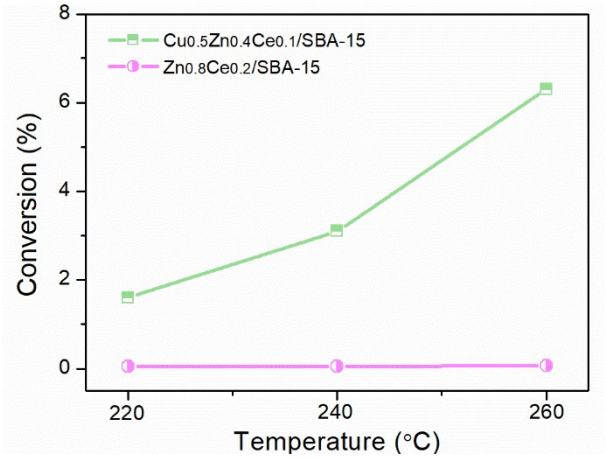

Fig. S7. The catalysis performances of the catalysts containing Cu or not. (H_2/CO_2 = 3, P = 3.0 Mpa, GHSV = 1200 h^{-1}).

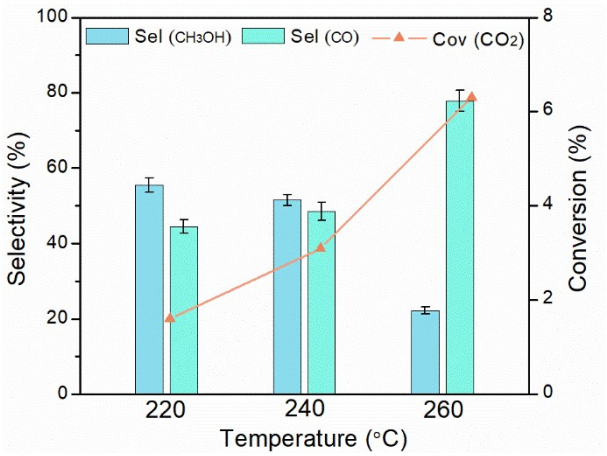

Fig. S8. The catalysis performances of $Cu_{0.5}Zn_{0.4}Ce_{0.1}$/SBA-15 catalysts with different reaction temperature. (Reaction conditions: H_2/CO_2 = 3, P = 3.0 MPa, GHSV = 1200 h^{-1}.)

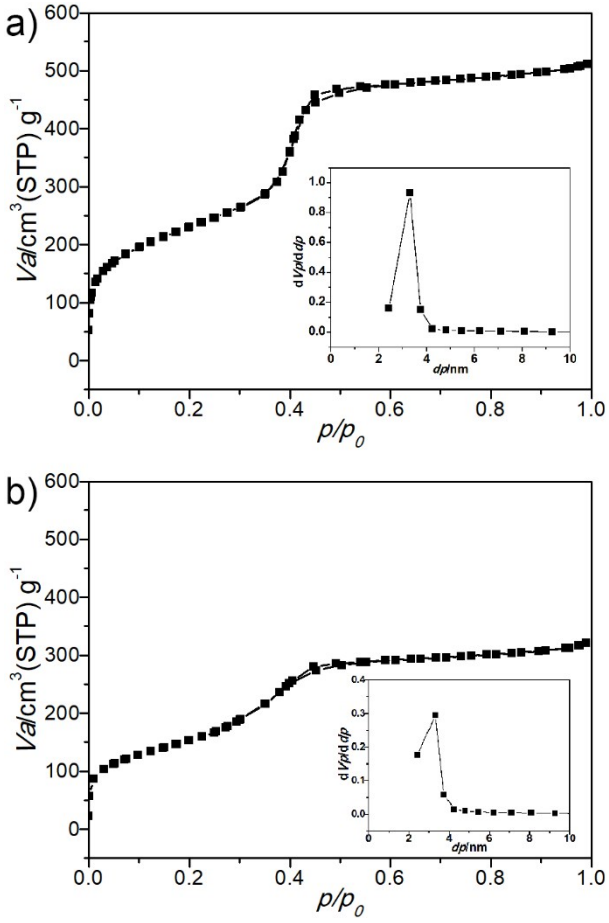

Fig. S9. N_2 adsorption-desorption isotherms and pore size distribution of MCM-41 (a) and MCM-41 supported $Cu_{0.5}Zn_{0.4}Ce_{0.1}$ catalysts (b).

Table S1. The particle size of Cu and CeO_x of the different catalysts.

Catalysts	Average particle size	
	Cu (nm)	CeO_x (nm)
$Cu_{0.5}Zn_{0.5}$/SBA-15	17.6	–
$Cu_{0.5}Zn_{0.4}Ce_{0.1}$/SBA-15	15.9	1.4
$Cu_{0.5}Zn_{0.25}Ce_{0.25}$/SBA-15	13.4	3.3
$Cu_{0.5}Zn_{0.1}Ce_{0.4}$/SBA-15	9.7	3.8
$Cu_{0.5}Ce_{0.5}$/SBA-15	–	4.4

Table S2. XPS integral values of Ce 3d.

Ce 3d	Peaks position	Area	Area %
v	882.2	1597.4	17.4
v′	884.6	972.2	10.6
v″	887.2	1227.9	13.4
v‴	900.7	1739.7	18.8
u	904.7	1198.3	12.9
u′	908.7	953.4	10.3
u″	913.2	538.4	5.8
u‴	917.7	1001.4	10.8

Table S3. Physical properties of different samples.

Catalysts	S_{BET} (m^2/g)	Pore size (nm)	Pore volume (cm^3/g)
MCM-41	821	3.3	0.76
$Cu_{0.5}Zn_{0.4}Ce_{0.1}$/MCM-41	585	3.3	0.46
SiO_2	341	3.8	0.49
$Cu_{0.5}Zn_{0.4}Ce_{0.1}/SiO_2$	138	21.3	0.53

Table S4. N_2O chemisorption uptakes of different samples under the same weight.

Catalysts	N_2O consumption·10^{-5} (μmol/g)
$Cu_{0.5}Zn_{0.4}Ce_{0.1}$/SBA-15	3.78
$Cu_{0.5}Zn_{0.4}Ce_{0.1}$/MCM-41	1.32
$Cu_{0.5}Zn_{0.4}Ce_{0.1}/SiO_2$	9.0
$Cu_{0.5}Zn_{0.4}Ce_{0.1}$	0.76

Active component ($Cu_{0.5}Zn_{0.4}Ce_{0.1}$) weight: 0.2 g.

Table S5. Catalysts mass used in catalytic evaluation tests.

Catalysts	Mass (g)
$Cu_{0.5}Zn_{0.5}$/SBA-15	1.58
$Cu_{0.5}Zn_{0.4}Ce_{0.1}$/SBA-15	1.64
$Cu_{0.5}Zn_{0.25}Ce_{0.25}$/SBA-15	1.69
$Cu_{0.5}Zn_{0.1}Ce_{0.4}$/SBA-15	1.69
$Cu_{0.5}Ce_{0.5}$/SBA-15	1.78

Table S6. The areas of desorption peaks in H_2-TPD and CO_2-TPD.

Samples	The desorption peaks area of H_2	The desorption peaks area of CO_2
$Cu_{0.5}Zn_{0.5}$/SBA-15	1.03	1.70
$Cu_{0.5}Zn_{0.4}Ce_{0.1}$/SBA-15	0.85	2.13
$Cu_{0.5}Ce_{0.5}$/SBA-15	0.23	1.73

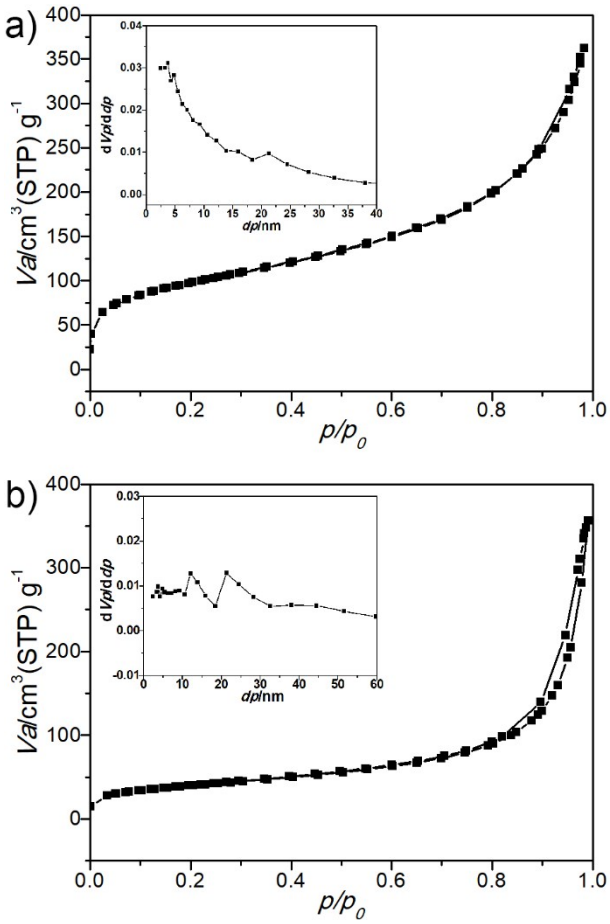

Fig. S10. N_2 adsorption-desorption isotherms and pore size distribution of SiO_2 (a) and SiO_2 supported $Cu_{0.5}Zn_{0.4}Ce_{0.1}$ catalysts (b).

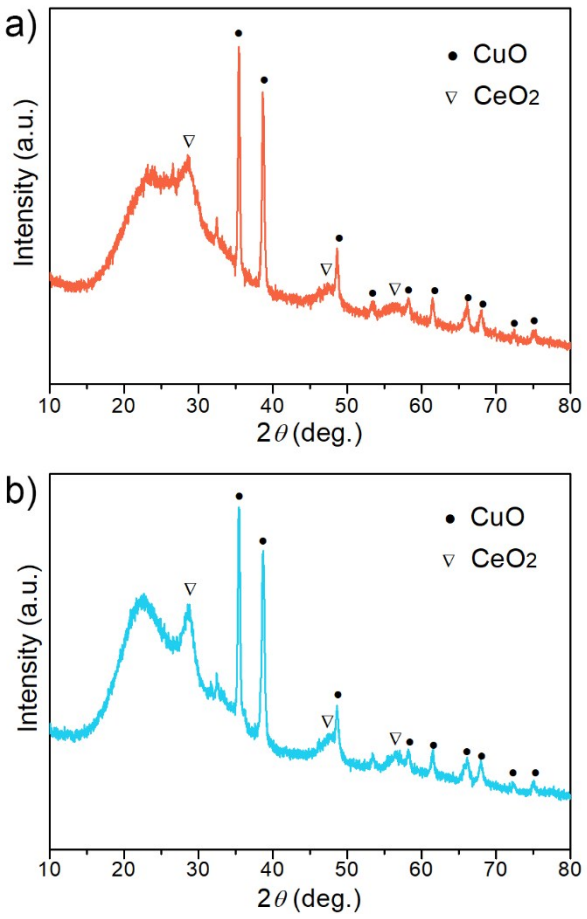

Fig. S11. XRD patterns of MCM-41 (a) and SiO_2 (b) supported $Cu_{0.5}Zn_{0.4}Ce_{0.1}$ catalysts.

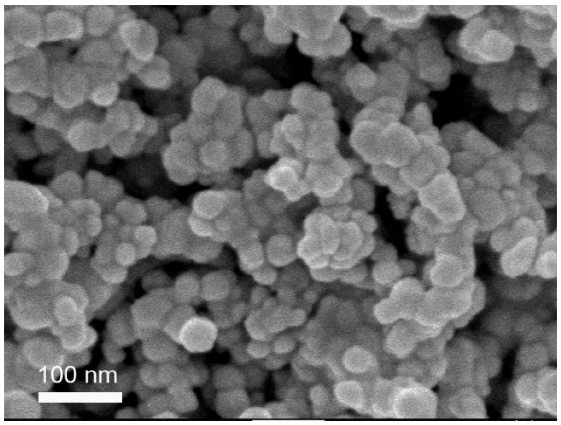

Fig. S12. SEM image of $Cu_{0.5}Zn_{0.4}Ce_{0.1}$ catalyst prepared by co-precipitation.

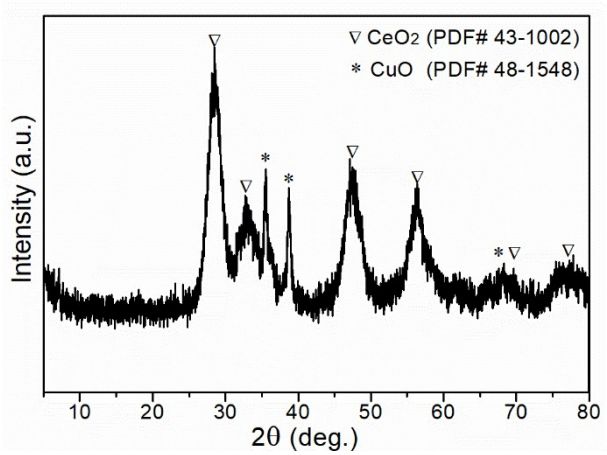

Fig. S13. XRD pattern of $Cu_{0.5}Zn_{0.4}Ce_{0.1}$ catalyst prepared by co-precipitation.

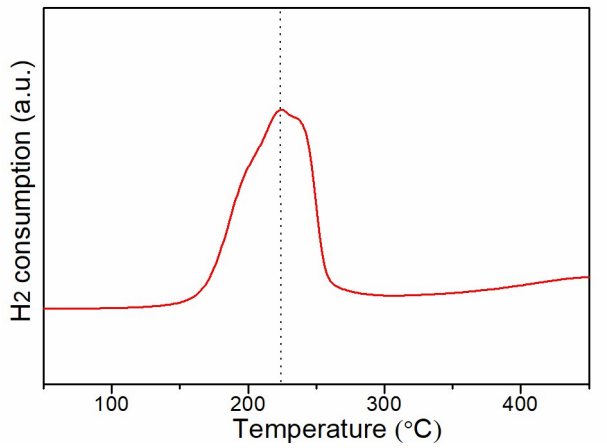

Fig. S14. H_2-TPR of $Cu_{0.5}Zn_{0.4}Ce_{0.1}$ catalyst prepared by co-precipitation.

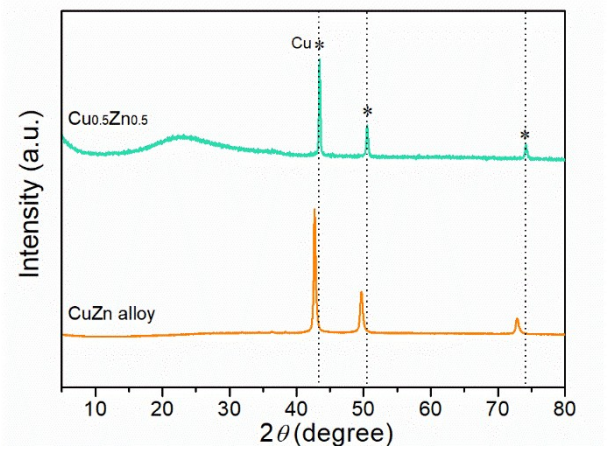

Fig. S15. XRD patterns of $Cu_{0.5}Zn_{0.5}$ catalyst and CuZn alloy.

Results and discussion

The particle size of Cu and CeO_x are calculated by Scherrer formula:

$$D = K\gamma/(B\cos\theta)$$

where K is the Scherrer constant (0.89); γ is the X-ray wavelength (0.154056 nm); B is the half-height width of the diffraction peak (rad); θ is the Bragg diffraction angle.

The obvious XRD peaks of CeO_2 and CuO are detected in MCM-41 and SiO_2 supported $Cu_{0.5}Zn_{0.4}Ce_{0.1}$ catalysts (Fig. S11), indicating that both the CeO_2 and CuO have an excellent crystallinity. In addition, ZnO is likely to exist in an amorphous form due to there is no related diffraction peaks are found in these catalysts.

As shown in Fig. S12, the $Cu_{0.5}Zn_{0.4}Ce_{0.1}$ catalyst prepared by co-precipitation method shows a relatively uniform particle size. The obvious XRD peaks of CeO_2 and CuO are found in Fig. S13, which suggests that both the CeO_2 and CuO have an excellent crystallinity. Of course, the amorphous ZnO is also present in the catalyst, which is confirmed by without the characteristic diffraction peaks of ZnO crystalline exist in the XRD pattern. H_2-TPR was used for detecting the reduction situation of catalyst (Fig. S14). The shoulder peak appeared at low temperature is attributed to the reduction of dispersed surface copper oxide species interacting with zinc oxide and cerium oxide. The shoulder peak appearing at high temperature are ascribed to the reduction of copper oxide species non-interacting with other oxides. The shoulder peaks are also the significant evidence that it come from the stepwise reduction of CuO species via Cu_2O to Cu metal.[1,2] There is no doubt that the copper oxide of the catalyst can be absolutely reduced to metal Cu at 300 °C.

As is observed from Fig. S15, the diffraction peaks of CuZn alloy are all shifted to a lower angle relative to the characteristic diffraction peaks of Cu (JCPDS card no. 04-0836). Thus, it is likely to be a reasonable explanation that during the calcination process, several Zn atoms have embedded into the Cu crystal, causing crystal lattice expansion as well as the crystal lattice spacing increase, which leads to the shift of the diffraction peaks to a smaller angle. XRD standard patterns of Cu and CeO_2 have been added to Fig.4b, it is observed that all the Cu diffraction peaks of the catalysts prepared in this work did not migrate, which indicates that there is no alloy formation in the $CuZnCeO_x$ aggregates. In addition, all the diffraction peaks of Cu and CeO_2 did not migrate, indicating that Cu could not make solid solutions inside the fluorite structure of ceria under the condition of catalyst preparation in this work. Thus, the phases of Cu, ZnO and CeO_2 coexists in the $CuZnCeO_x$ aggregates.

It is displayed in Fig. S16 that the three-dimensional schematic diagram of catalytic evaluation device and on-line gas chromatographic analysis system.

Fig. S16. 3D illustration of the device about CO_2 catalytic evaluation and online detection.

Computational details of DFT

All DFT calculations were performed using the Vienna Abinitio Simulation Package (VASP).[3,4] The exchange and correlation effects were treated by the generalized gradient approximation (GGA) with Perdew-Burke-Ernzerhof (PBE) functional to describe weak interactions.[5] Electron-ion interactions were described by the projector-augmented plane-wave (PAW) method.[6,7] A plane-wave kinetic energy cutoff of 550 eV was adopted to treat the valence electrons. 3 × 3 × 1 Monkhorst-Pack mesh was used for all geometry optimizations and 5 × 5 × 1 Monkhorst-pack mesh was used to calculate the total energy of system. The convergent of energy and forces were set to 1×10^{-5} eV and 0.05 eV/Å. The DFT + U methodology was used to treat the on-site Coulomb and exchange interaction of the strongly localized Ce 4f electrons with an effective U = 5.0 eV.[8-10] The van der Waals dispersion forces were considered using the zero damping DFT-D3 method of Grimme to account for the weak interactions between adsorbates and surfaces.[11]

References:

[1] K. Chang, T. Wang, J. G. Chen, *Appl. Catal. B*, 2017, **206**, 704–711.

[2] S. Natesakhawat, J. W. Lekse, J. P. Baltrus, P. R. Ohodnicki, B. H. Howard, X. Deng, C. Matranga, *ACS Catal*., 2012, **2**, 1667–1676.

[3] G. Kresse, J. Furthmüller, *Comput. Mater. Sci*., 1996, **6**, 15–50.

[4] G. Kresse, J. Furthmüller, *Phys. Rev. B*, 1996, **54**, 11169–11186.

[5] J. P. Perdew, K. Burke, M. Ernzerhof, *Phys. Rev. Lett*., 1996, **77**, 3865−3868.

[6] P. E. Blöchl, *Phys. Rev. B*, 1994, **50**, 17953–17979.

[7] G. Kresse, D. Joubert, *Phys. Rev. B*, 1999, **59**, 1758–1775.

[8] V. I. Anisimov, J. Zaanen, O. K. Andersen, *Phys. Rev. B: Condens. Matter Mater. Phys*., 1991, **44**, 943−954.

[9] S. L. Dudarev, G. A. Botton, S. Y. Savrasov, C. J. Humphreys, A. P. Sutton, *Phys. Rev. B: Condens. Matter Mater. Phys*., 1998, **57**, 1505−1509.

[10] S. Fabris, G. Vicario, G. Balducci, S. de Gironcoli, S. Baroni, *J. Phys. Chem. B*, 2005, **109**, 22860−22867.

[11] S. Grimme, J. Antony, S. Ehrlich, H. Krieg, *J. Chem. Phys*., 2010, **132**, 154104.